

Document downloaded from:

<http://hdl.handle.net/10251/204094>

This paper must be cited as:

Frasci, E.; Novella Rosa, R.; Pla Moreno, B.; Arsie, I.; Jannelli, E. (2023). Investigation of the benefits of passive TJI concept on cycle-to-cycle variability in a SI engine. *International Journal of Engine Research*. 24(8):3359-3357. <https://doi.org/10.1177/14680874221149115>



The final publication is available at

<https://doi.org/10.1177/14680874221149115>

Copyright SAGE Publications

Additional Information

This is the author's version of a work that was accepted for publication in *International Journal of Engine Research*. Changes resulting from the publishing process, such as peer review, editing, corrections, structural formatting, and other quality control mechanisms may not be reflected in this document. Changes may have been made to this work since it was submitted for publication. A definitive version was subsequently published as <https://doi.org/10.1177/14680874221149115>.

Investigation of the benefits of passive TJI concept on cycle-to-cycle variability in a SI engine

Emmanuele Frasci¹ , Ricardo Novella Rosa² , Benjamín Plá Moreno² , Ivan Arsie¹ and Elio Jannelli¹

Abstract

During the last years, the sales of vehicles equipped with Spark-Ignition (SI) engines have increased, to the detriment of those powered by Compression-Ignition (CI) engines. However, SI engines provide lower efficiency than CI engines, due to the low compression ratio and stoichiometric mixture operation. A way to increase the efficiency of SI engines is lean combustion, as it allows to increase the specific heats ratio (γ) and reduces pumping losses at part loads. Nevertheless, the operation with extremely lean mixtures deals with ignition issues, promoting Cycle-to-Cycle Variability (CCV) and increasing the probability of misfire. The prechamber ignition concept, also known as Turbulent Jet Ignition (TJI), is a promising solution for enabling the implementation of lean combustion, without its drawback in SI engines. Such a concept can be implemented according to two approaches: In active TJI, there is an additional fuel supply system inside the prechamber, while in passive TJI there isn't. Therefore, the main advantage of passive TJI is its simplicity, as the prechamber can be installed into a conventional spark plug body, with obvious benefits in terms of packaging and costs. In this work, the benefits of passive TJI on combustion and performance are assessed by simulation analyses. Particularly, a 1-D engine model was developed to simulate the TJI combustion and was validated versus experimental data. Afterward, a 0-D method was applied to assess the impact of the relative air-fuel ratio on CCV. The analysis was carried out in a high speed and load operating condition, namely 4500 rpm and 13 bar of IMEP, under both stoichiometric and lean mixture. Experimental and numerical results demonstrate the effectiveness of the passive TJI concept in promoting faster and more stable combustion also in lean-burn conditions.

Keywords

Passive turbulent jet ignition, lean combustion, engine modeling, combustion modeling, cycle-to-cycle variability analysis

Introduction

During the last years, an important change in passenger car sales in the European Union occurred. The sales of vehicles equipped with Compression-Ignition (CI) engines fell and its main competitor, namely the Spark-Ignition (SI) engine, has taken up the market share left. This is partially ascribable to the extra cost of the after-treatment system of CI engines, needed to satisfy the extremely restrictive European emission standards.¹ However, SI engines suffer from lower efficiency, and then lower fuel economy, if compared to CI engines.² This is ascribable to the low compression ratio, due to the fuel octane number and the intrinsic knock tendency,^{3,4} and the need to operate the engine with a stoichiometric air-fuel ratio (i.e. $\lambda = 1.0$). The stoichiometric air-fuel ratio limitation is needed to guarantee

an adequate flame front velocity⁵ and the use of the Three-Way Catalyst (TWC) to control pollutant emissions.⁶ An attractive solution to improve the efficiency of SI engines is lean combustion, which consists in operating the engine with a relative air-fuel ratio higher than the stoichiometric value (i.e. $\lambda > 1$).⁷ Lean burn operation allows for increasing engine efficiency due to

¹Department of Engineering, University of Naples "Parthenope," Napoli (NA), Italy

²CMT – Motores Térmicos, Universitat Politècnica de València, Valencia, Spain

Corresponding author:

Emmanuele Frasci, Department of Engineering, University of Naples "Parthenope," Centro Direzionale – Isola C4, Napoli (NA) 80143, Italy. Email: emmanuele.frasci001@studenti.uniparthenope.it

the reduction of heat losses through the combustion chamber walls, the increase of the specific heats ratio (γ), and the reduction of pumping losses at part loads.⁸ On the other hand, the use of extreme lean mixtures results in ignition and flame propagation issues,⁹ promoting the Cycle-to-Cycle Variability (CCV) and increasing the probability of misfire that in turn dramatically impacts on HC emissions.¹⁰ The origin of CCV has been investigated in d'Adamo et al.¹¹ through Large Eddy Simulation, while in Maldonado and Kaul¹² and Maldonado et al.¹³ control-oriented approaches to capture the correlation between cycle-to-cycle combustion variability and the misfire limit in SI engines under high EGR levels are described. Pla et al.¹⁴ propose a control-oriented combustion model able to characterize the CCV, either in steady state or in transient conditions.

The prechamber ignition concept, also known as Turbulent Jet Ignition (TJI),^{15–17} is a promising solution to implement the aforementioned strategies while overcoming their drawbacks in SI engines.^{18,19} This ignition concept adopts a conventional spark plug to ignite a given quantity of air/fuel mixture in a dedicated volume (the prechamber), which is connected to the combustion chamber (the main chamber) through a set of orifices.²⁰ The combustion process causes a pressure increase inside the prechamber, so a set of turbulent and reacting jets are ejected toward the main chamber, forcing the combustion onset in multiple locations.²¹

The details of the complex characteristics of the turbulent jets have been discussed in Chinnathambi et al.²² and Biswas et al.²³ The kinematics and development of the reacting jets were studied by Allison et al.²⁴ In suitable conditions, the TJI concept promotes very fast main chamber combustion and lower CCV if compared to a traditional spark-ignition system.²⁵ This is due to the greater initial flame area promoted by the turbulent reacting jets ejected from the prechamber, which leads to faster flame development within the main chamber also under lean mixture. The shortening of the first stage of combustion increases the stability of engine operation. Moreover, faster combustion is also favorable to reduce the knock tendency, thus allowing to increase in the compression ratio to further improve engine efficiency.²⁶

The TJI concept can be implemented in two different ways, namely active and passive.^{15,16} In active TJI,²⁷ there is an additional fuel supply system inside the prechamber that allows controlling the air-fuel ratio close to the stoichiometric value, regardless of the value assumed in the main chamber.

Other benefits of the active TJI systems are charge stratification and the reduction of HC and NOx emissions.²⁸

In passive TJI systems,²⁹ there is no additional fuel supply inside the prechamber, so the air-fuel ratio cannot be directly controlled therein. On the other hand, passive TJI systems are very simple, as the prechamber can be directly mounted into a conventional spark plug

Table 1. Engine technical data.

Engine	Four-stroke SI
Number of cylinders [-]	1
Displacement [cm ³]	404
Bore–Stroke [mm]	80.0–80.5
Compression ratio (geometric) [-]	13.4:1
Valvetrain [-]	DOHC
Number of valves/cylinder [-]	2 intake, 2 exhaust
Fuel injection system [-]	PFI ($p_{inj, max} = 6$ bar)

body. Therefore, passive TJI offers undoubtedly advantages in terms of packaging and low costs. However, the prechamber filling and scavenging, which depends on the mass transfer between the two chambers, together with limits of the concept in terms of maximum air and/or EGR dilution, should be still investigated.

In this paper, the experimental and numerical analysis of the effects of the passive TJI system on the combustion process both in stoichiometric and lean-burn operating conditions is presented. First, a 1-D engine model was developed to simulate the combustion process, considering the dynamics of the turbulent reactive jets from each prechamber nozzle and the subsequent flame front propagation.³⁰ At this stage, the model validation was carried out by comparison with experimental data, measured at the test bed on a single-cylinder SI engine equipped with a passive prechamber. The tests were performed at 4500 rpm, increasing λ from 1.0 to 1.6, to assess the benefits of the passive TJI concept under lean mixture conditions. Furthermore, the clustering of the acquired cycles was carried out for different λ values, to investigate the relative importance of the CCV for different air-fuel ratios.

Afterward, a stochastic methodology was presented and applied to estimate the influence of CCV under different air dilution conditions, making use of the 1-D model simulation results. The results of CCV prediction are validated against the experimental data. Furthermore, the capability of such an approach to predict the CCV even in case of lack of experimental data is also assessed and discussed.

In this work, the k-means algorithm, like in Novella et al.,³¹ is used to group the registered cycles and classify them into different categories, including misfiring and knocking cycles. Such classification is useful to perform a stochastic prediction of the CCV.

Experimental layout

Engine and test bench characteristics

The experimental campaign was carried out on a single-cylinder research four-stroke turbocharged SI engine, well representative of those currently employed in passenger cars. The most important engine data are listed in Table 1.

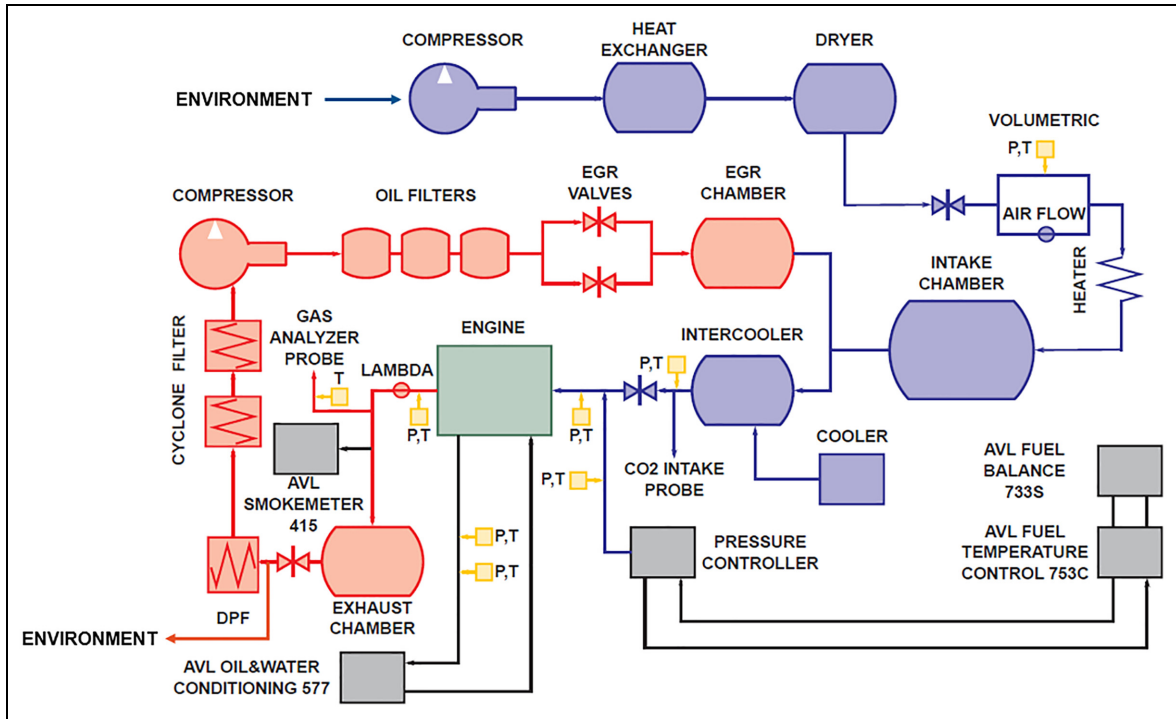


Figure 1. Complete layout of the engine test bench.³²

A Port Fuel Injection (PFI) system, assembled in the intake manifold at 270 mm from the cylinder head, is adopted to generate a homogeneous air-fuel mixture. The cylinder head is equipped with four valves, with double-overhead camshafts (DOHC), to improve the scavenging process, since the valve overlap is removed to avoid short-circuit losses.

The engine is assembled into a fully instrumented test bench, represented in Figure 1.

Compressed air is provided by an external compressor to simulate boost pressure, while the exhaust back-pressure is reproduced and controlled through a throttle valve installed in the exhaust line.³² The test bench is also equipped with a low-pressure EGR system, designed to provide arbitrary levels of cooled EGR at any intake pressure.

During the tests, a calibrated gasoline with 95 Research Octane Number (RON95) is used. The fuel consumption is measured by an AVL 733 gravimetric dynamic fuel meter while the fuel temperature is controlled by an AVL 753 conditioner.

Emissions of CO, CO₂, O₂, HC, and NO_x are measured by a Horiba MEXA 7100 gas analyzer while soot emissions are measured by an AVL 415 Smoke meter. The mean air-fuel ratio is calculated by an air flow meter and fuel balance measurements.

In-cylinder air-fuel ratio is measured by the Horiba MEXA 7100 gas analyzer and by a UEGO sensor mounted in the exhaust line.³²

In-cylinder pressure is measured by a piezoelectric sensor, while intake and exhaust pressures are measured by piezoresistive sensors. For all frequency signals, a

sampling resolution of 0.2°CA is adopted. During the experimental campaign, 250 cycles are acquired for all the operating conditions investigated. Further details on the engine test bench are given in Benajes et al.³²

Prechamber description

During the experimental campaign, a passive prechamber is used in place of the conventional spark plug. Such prechamber is designed to be placed in the same housing in the cylinder head of the conventional spark plug, being easy and quick to exchange between concepts and/or prechambers. The location of the passive prechamber in the cylinder head is represented in Figure 2.

The geometrical data of the prechamber used for this work are listed in Table 2.

The choice of this design as a reference came from a comparison between two passive prechambers performed in Benajes et al.³² Such design demonstrated to have better performance in terms of jet penetration than the other prechamber tested, which was characterized by a lower A/V ratio.

Operating conditions

In this work, an operating condition at high engine speed (4500 rpm) and high load (around 13 bar IMEP) was considered. The reason behind this choice lies in the fact that high speeds compromise the scavenging and filling of the prechamber, which is critical in passive configurations as discussed in the introduction.

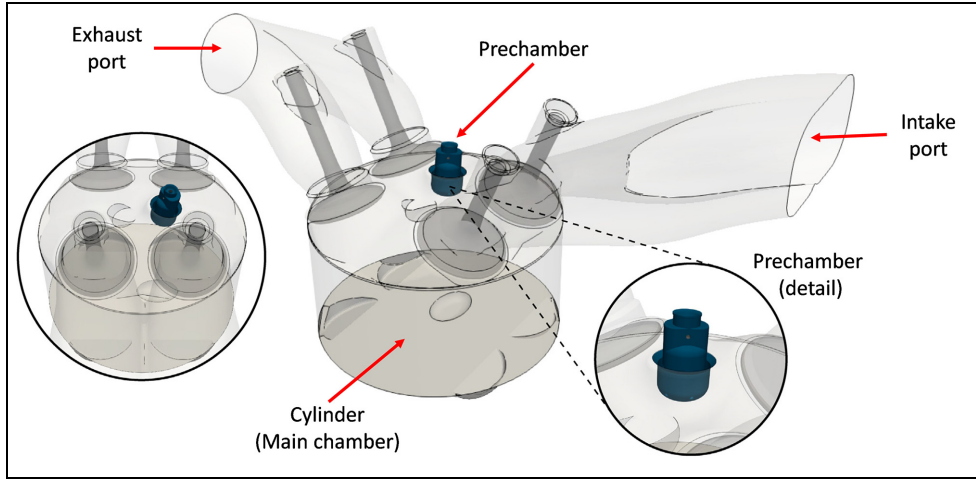


Figure 2. Representation of the engine design, including the passive prechamber positioning in the cylinder head.³²

Table 2. Main geometrical features of the passive prechamber.

Volume [mm ³]	600
Hole diameter [mm]	0.7
Number of holes [-]	6
A/V [1/m]	3.9

Table 3. Operating conditions investigated.

	$\lambda = 1.0$	$\lambda = 1.2$	$\lambda = 1.4$	$\lambda = 1.6$
Engine speed [rpm]	4500	4500	4500	4500
IMEP [bar]	12.7	13.2	13.3	12.6
Injected fuel [mg/cycle]	28.5	28.5	28.5	28.5
Intake air temperature [K]	289.86	291.75	292.91	294.58
Intake pressure [bar]	1.101	1.292	1.501	1.720
Exhaust pressure [bar]	1.062	1.206	1.386	1.531
Coolant and oil temperature [K]	350	350	350	350

The high load was selected to investigate the impact of the passive TJI concept on the knock tendency, at different air-fuel ratios. The tests are carried out at different λ values, by keeping the injected fuel quantity per cycle constant and increasing the air flow rate by controlling the intake manifold pressure. Moreover, the EGR rate was set to 0% for all the operating conditions investigated.

The details of the operating conditions investigated are listed in Table 3.

Engine model development

A 1-D model of the experimental facility and the single-cylinder engine, described in section 2, was developed by using the commercial software GT-Power.³³ Since the intake and exhaust systems were included within the

model, the whole engine cycle was simulated. Therefore, it was also possible to assess the cylinder scavenging process. Moreover, the sub-models embedded in the engine model allowed the simulation of various processes, like combustion and heat transfer.

However, particular attention was paid to the development of the combustion sub-model, described in the following.

Combustion sub-model

The prechamber combustion is simulated by a Wiebe function,^{30,34} whose tuning was performed by matching the prechamber CA50 with the main chamber Start Of Combustion (SOC) and imposing the value of the prechamber combustion duration for each λ since no experimental data on the prechamber were available. Particularly, the prechamber combustion duration is fixed at 4°CA for the cases with $\lambda = 1.0$ and 1.2, at 5°CA for $\lambda = 1.4$, and 6°CA for $\lambda = 1.6$, according to 3D-CFD simulation results presented in Novella et al.³⁵

In the cylinder, the combustion process is simulated through a multi-zone predictive model, which describes the evolution and burning of the turbulent reactive jet and the subsequent flame front propagation.

Initially, a single thermodynamic zone, the main unburned zone, contains all the mass in the cylinder. The fresh charge from the intake ports is added to this zone. The main unburned zone exchanges mass and energy with the prechamber through its orifices. Once the combustion starts in the prechamber after the spark time, a new thermodynamic zone, namely the jet zone, develops in the cylinder from each prechamber orifice. The jet dynamics inside the main chamber are governed by two quantities, namely the penetration distance (t) and the tip velocity $u(t)$ ³⁶:

$$S(t) = C_s t^{1/2} \left(\frac{u_{noz} d_{noz}}{C_d} \sqrt{\frac{\rho_{noz}}{\rho_{cyl}}} \right)^{1/2} \quad (1)$$

$$u(t) = C_u t^{-1/2} \left(\frac{u_{noz} d_{noz}}{C_d} \sqrt{\frac{\rho_{noz}}{\rho_{cyl}}} \right)^{1/2} \quad (2)$$

where t is the elapsed time [s], u_{noz} is the velocity at the prechamber nozzle [m/s], d_{noz} is the nozzle diameter [m], C_d is the nozzle discharge coefficient, ρ_{noz} is the fluid density inside the jet at the nozzle exit, and ρ_{cyl} is the density of the charge inside the main chamber [kg/m³]. C_s and C_u are model parameters. As the jet enters the cylinder, it expands and slows down by entraining mass from the surrounding fluid. Considering the momentum conservation, the mass entrained by the jet is given by:

$$m_{je}(t) = C_e m_{noz} \left(\frac{u_{noz}}{u(t)} - 1 \right) \quad (3)$$

where m_{noz} is the mass in the jet at the prechamber nozzle exit [kg] and C_e is the entrainment rate multiplier, a model parameter that considers transient effects in the entrainment process which are not explicitly modeled.^{33,34} The mixture entrained by the jet undergoes an ignition delay modeled by an Arrhenius-like equation, which can be modified by the ignition delay multiplier C_i .^{33,34} A fraction of the charge entrained by the jet is set aside for premixed combustion, whose rate is controlled by the chemical kinetics and can be adjusted by the premixed combustion rate multiplier C_{pm} .³³

After the ignition, the jet continues to entrain mass based on equations (1)–(3). The burn rate inside the jet (dm_{jb}/dt) is calculated as follows^{33,34}:

$$\frac{dm_{jb}}{dt} = C_{df} m_{ju} \frac{\sqrt{k}}{V_{cyl}^{1/3}} f([O_2]) + \dot{s}_f m_{ju} \quad (4)$$

$$\frac{dm_{ju}}{dt} = \frac{dm_{je}}{dt} - \frac{dm_{jb}}{dt} \quad (5)$$

$$\dot{s}_f = \frac{1}{m_u} \frac{dm_{jb}}{dt} \quad (6)$$

where m_{je} is the mass entrained by the jet [kg], m_{ju} and m_{jb} are the unburned and the burned mass inside the jet, respectively, m_u is the total unburned mass in the main chamber, k is the turbulent kinetic energy [m²/s²], V_{cyl} is the cylinder volume [m³], and C_{df} is the diffusion combustion multiplier. The term $\frac{\sqrt{k}}{V_{cyl}^{1/3}} f([O_2])$ is a mixing-

controlled burn rate, that depends on the turbulence level in the cylinder and the stoichiometry of the mixture in the reactive jet.³³ The function $f([O_2])$, dependent on the oxygen concentration, determines a burn rate reduction due to reduced oxygen amount. Finally, \dot{s}_f is a source term that couples the jet combustion with the flame propagation, as part of the mass entrained by the jet can be entrained and burned by the flame front. m_{jb} is the mass burned behind the flame front.

Once the jet is fully developed, a turbulent spherical flame front is initiated at the jet tip, whose propagation is modeled as a turbulent entrainment process, followed by combustion.^{37,38} The flame front is initiated at a

fixed location inside the main chamber and there are many flame kernels as the number of turbulent reactive jets. During its propagation, the flame front entrains mass from the main chamber, which is burned with a characteristic timescale. Such phenomenon is modeled by the following equations^{33,34}:

$$\frac{dm_{fu}}{dt} = \rho_u A_e S_T - \frac{dm_{fb}}{dt} \quad (7)$$

$$\frac{dm_{fb}}{dt} = \frac{m_{fu}}{\tau} + \dot{s}_j m_{fb} \quad (8)$$

$$\tau = C_{tls} \frac{\lambda}{S_L}; \dot{s}_j = \frac{1}{m_b} \frac{dm_{fb}}{dt}; S_T = S_L + C_{tfs} u' \quad (9)$$

where equation (7) governs the entrainment rate of the mixture in the main chamber by the flame front and equation (8) governs the burning rate of the entrained mass. m_{fu} is the unburned mass entrained by the flame front, ρ_u is the unburned mixture density, A_e is the entrainment surface area, S_L and S_T are the laminar flame speed and the turbulent flame speed, respectively (their calculation is shown in GT-Suite Engine performance application manual, Gamma Technologies³³), τ is the burning characteristic timescale and \dot{s}_j is a source term coupling the flame propagation model with the jet combustion model. In fact, part of the mass entrained by the flame front can be entrained and burned by the jet. The time constant τ and the turbulent flame speed S_T depend on the turbulence intensity u' and the Taylor microscale $\lambda = L_i / Re_T$, where L_i is the turbulence integral length scale and Re_T is the turbulent Reynolds number. L_i and u' , in their turn, are calculated by the turbulence sub-model in the main chamber.³⁹ The flame front propagation model tuning parameters are the dilution effect multiplier C_{de} , which takes into account the dilution of the fresh charge by residual gases and acts on S_L , the turbulent flame speed multiplier C_{tfs} , which instead act on S_T , and the Taylor length scale multiplier C_{tls} , which acts on the Taylor microscale of the turbulence, that influences the time constant of the combustion process τ (equation (9)).³³

Heat transfer sub-model

The heat transfer in the main chamber is simulated by a modeling approach based on the Woschni heat transfer coefficient correlation.⁴⁰ More details about the simulation of heat transfer in both the prechamber and main chamber are given in Frasci et al.³⁰

CCV prediction and modeling

To investigate the relative importance of the CCV, the 250 in-cylinder pressure cycles, acquired for each operating condition experimentally investigated, are classified by a k-means clustering methodology. It divides a data set into a certain number of distinct clusters by grouping the observations with similar predefined characteristics. K-means was chosen, as it is one of the

easiest to implement machine learning algorithms, guarantees a quick convergence, and can be easily generalized. Moreover, the k-means algorithm can deal with very large datasets and is efficient in terms of its computational cost, and its results can be easily interpreted. K-means is an unsupervised classification algorithm that provides a number of clusters (k) and a set of characteristics (defining the dimensions of space) and divides a dataset in k groups by minimizing the distance between the elements of a cluster and its mean in the considered space. The interested reader can find a deep description of the algorithm in the paper of Lloyd,⁴¹ or in the more recent review about k-means and applications.⁴²

K-means algorithm has three main steps: (i) initialization, (ii) assignment, and (iii) update.³¹

In the first step, once the number of clusters (K) is set, an initial centroid ($c_i, i = 1, \dots, K$) for each cluster is defined.

In the second step, each sample of the data set is assigned to the cluster with the nearest centroid. For a given data set $\{x_1, x_2, \dots, x_N\}$, the algorithm searches for the position of the centroids that minimizes the objective function, given by:

$$J = \sum_{i=1}^K \sum_{j=1}^N x_j - c_i \quad (10)$$

where $x_j - c_i$ is the Euclidean distance between the generic observation of the data set x_j and the centroid c_i of the i -th cluster.

In the third step, the centroids c_i are updated.

In the present work, the clustering of the experimental data is carried out by considering three thermodynamic variables characterizing the combustion process, namely the maximum Heat Release Rate (HRR), the combustion duration (CA95-CA5), and the combustion phasing (CA50).

Firstly, the pressure cycles characterized by abnormal combustion events, namely misfire and knock, are separated from the cycles in which normal combustion is observed. Particularly, cycles in which the max HRR is below 20 J/deg are assigned to the misfiring cluster, while cycles in which the Maximum Amplitude of Pressure Oscillations (MAPO) is above a certain threshold are assigned to the knocking cluster. For all the cycles, MAPO calculation is performed by applying a band-pass filter to the in-cylinder pressure signal, to isolate the high frequencies oscillations of the signal.⁴³ The band-pass frequency range was chosen between 4 and 27 kHz. The MAPO threshold to identify the knocking cycles was chosen for each λ value according to the observed amplitude of high-frequency pressure signal oscillations.

Once misfiring and knocking cycles are isolated, cycles with normal combustion are grouped into two clusters, namely slow-burning and fast-burning cycles, by using the aforementioned k-means algorithm. Therefore, the cycles acquired in the engine test bench

are grouped in four clusters. In any case, the proposed methodology to model the Cycle-to-Cycle Variability (CVV) is completely general and can be extended to a higher number of clusters.

Once the division of all the 250 cycles in four clusters (misfiring cycles, slow cycles, fast cycles, and knocking cycles) is performed, the mean cycle for each cluster is obtained. At this point, the most interesting thermodynamic variables related to the mean cycle belonging to each cluster are collected, and a particular set of combustion model parameters is identified for any of the clusters.

The previous classification is then used to model the CVV in a stochastic way. To this aim, any cycle to be simulated will be allocated according to some probabilistic variable in one of the four clusters. Particularly, the choosing of the cluster for the first cycle is carried out by considering the total probability of each cluster, estimated from the frequency of this cluster in the experimental data according to the following equation:

$$prob(i) = \frac{n_i}{n_{tot}} \quad (i = 1, \dots, K) \quad (11)$$

where n_i is the number of cycles in the i -th cluster, n_{tot} is the number of all the acquired cycles and K is the number of clusters in which the experimental data have been grouped.

Once the probability of each cluster is determined, the objective is to generate a random number according to the corresponding probability distribution (equation (11)). To this aim, a homogeneously distributed random number between 0 and 1 is generated and the interpolation of the obtained number in the cumulated probability for the four clusters leads to the selection of a cluster according to the desired distribution.

In a further step, the subsequent cycles are allocated in the four clusters based on the conditioned probability of each cluster. Particularly, a matrix of the probability of each cluster is computed, where each element $p_{i,j}$ ($i, j = 1, \dots, K$) represents the probability of a cycle to be in the j -th cluster if the previous cycle is allocated in the i -th cluster. Then, the same process used to allocate the first cycle is repeated but, in this case, using the probability conditioned by the previous cycle. So, each cycle is allocated in one of the four clusters based on the cluster chosen for the previous cycle, assuming that the cycle allocation is a Markov process. A scheme of the procedure adopted to assess the CCV is depicted in Figure 3.

In this way, it is possible to obtain a sequence of all the relevant thermodynamic variables characterizing the engine performance and the combustion process and compare them with those observed from the experimental data.

Model parameters' identification

According to the previous section, there are seven tuning parameters in the predictive combustion model, namely C_e , C_i , C_{pm} , C_{df} , C_{de} , C_{ifs} , and C_{tfs} , plus the

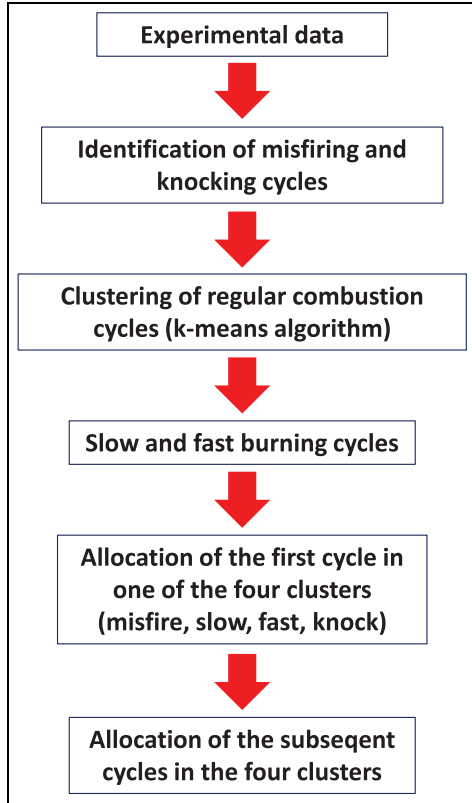


Figure 3. Schematic representation of the approach adopted to model the CCV.

prechamber combustion duration. Their identification was carried out by using a genetic algorithm-based optimization procedure, that minimizes the root mean square error between the measured and predicted heat release rates. Particularly, each case was optimized independently, and a different set of tuning parameters was identified for each λ value. In a further step, the mean value of C_{df} , C_{tfs} , and C_{tls} over all the four cases was imposed for each λ value, as their values showed to be almost constant with λ . In fact, those parameters affect the turbulence inside the jet (C_{df}) and in the main chamber (C_{tfs} and C_{tls}), which is more influenced by the engine speed than by the mixture composition (i.e. λ).

Once the model was validated versus the mean cycle of each case, further validation was carried out against the mean cycle of the different clusters. To do this, slight modifications to the tuning constants' values found for the mean cycles of each case were applied. Particularly, the values of C_{tfs} and C_{tls} were slightly varied with respect to those adopted for the mean cycle of each case, given that one of the main sources of the CCV is the stochastic nature of the turbulent flow field inside the cylinder.

Results and discussion

Combustion model validation

Combustion model validation was carried out by comparing simulation results and experimental data for the

engine operating conditions listed in Table 3. One of the purposes of this work is to assess the model's accuracy in predicting the effects of mixture leaning out on the combustion process, in a medium-to-high speed and load condition. Figure 4(a)–(h) shows the comparison of in-cylinder pressure and net HRR traces.

Observing the in-cylinder pressure traces (Figure 4(a), (c), (e), and (g)), an increase of the maximum pressure, together with its shift toward the Top Dead Center (TDC), can be noted as λ is swept from 1.0 to 1.6. The former is due to the increase of intake pressure to obtain the mixture leaning, while the latter is due to the higher spark timing. However, the mixture leaning results, as expected, in a slowdown of the combustion process, evidenced by the significant reduction of maximum HRR as λ increases (Figure 4(b), (d), (f), and (h)). This is ascribable to the laminar flame speed reduction as the mixture becomes leaner, due to the higher relative importance assumed by heat losses with respect to the energy released by fuel combustion.² Furthermore, the increase of the air-fuel ratio results also in a slowdown of jet combustion, as it can be noted by the reduction of the initial slope of the HRR traces. This trend is more evident when λ is swept from 1.2 to 1.6. This is due to the advancing of the spark timing as λ is increased, which results in a reduction of the fuel mass trapped inside the pre-chamber at the Start of Combustion (SOC), which in turn leads to a reduction of the energy available for the ejection and a lower jet penetration.

However, the adoption of a passive TJI concept allows guaranteeing a faster combustion process with respect to a conventional spark ignition system, particularly in the case of lean mixture, thus resulting in higher in-cylinder pressure.³² This is due to the greater initial flame area promoted by the turbulent reactive jets, which leads to a faster flame development within the main chamber if compared to a conventional SI.

The previous figure evidences a good agreement of the simulation results with the experimental data. However, the maximum in-cylinder pressure is slightly overestimated by the model in the cases with $\lambda = 1.4$ and 1.6 (Figure 4(e) and (g)). On the other hand, a very slight underestimation of maximum in-cylinder pressure can be observed in cases with $\lambda = 1.0$ and 1.2 (Figure 4(a) and (c)). This is due to the assumption to use the same tuning parameters related to the flame propagation, namely C_{tfs} and C_{tls} , for all the test cases. Being the values chosen for these tuning parameters an average over all the investigated cases, this behavior of the model in predicting combustion is expected.

Moreover, the predicted maximum HRR is more shifted toward the expansion stroke than the experimental one. Particularly, the value of the predicted maximum HRR is slightly lower than the experimental one in the test cases with $\lambda = 1.0$ and 1.2 (Figure 4(b) and (d)), denoting a slower flame front propagation in the cylinder. This is still due to the assumption to keep

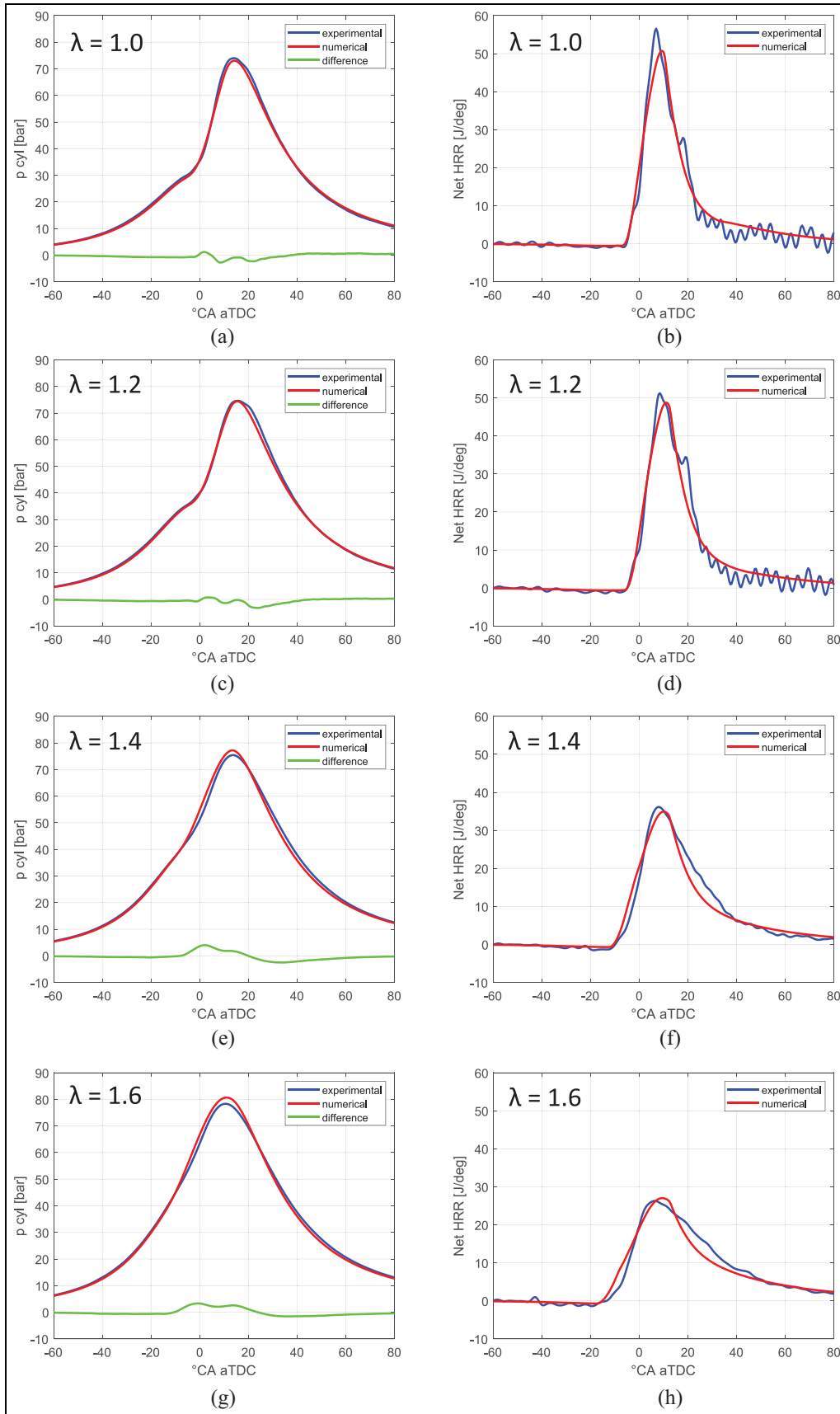


Figure 4. (a-h) Comparison between the experimental and numerical in-cylinder pressure and net HRR traces at 4500 rpm, for different λ values.

Table 4. Values of the COV_{IMEP} and MAPO for different air-fuel ratios.

Engine speed [rpm]	λ [-]	COV_{IMEP} [%]	MAPO [bar]
4500	1.0	0.75	1.55
4500	1.2	9.58	2.37
4500	1.4	9.99	0.59
4500	1.6	5.94	0.24

the same values of C_{tfs} and C_{tls} for all the investigated cases.

Other differences between the experimental and the predicted HRR can be found in the cases with $\lambda = 1.4$ and 1.6 (Figure 4(f) and (h)), in the first phase of main chamber combustion. Particularly, the initial slope of the simulated HRR trace seems to be higher than the experimental result, denoting a slight overestimation of the jet combustion velocity.

CCV analysis

Clustering of the experimental data. The results of the clustering analysis to evaluate and predict the impact of air-fuel ratio on CCV are presented in this section. The cases with $\lambda = 1.0$ and 1.4 are firstly analyzed, as they correspond to the operating conditions with the lowest and the highest CCV, respectively (Table 4).

It is worth noting that, in every case, the COV_{IMEP} is below 10%, which is considered the upper threshold for combustion stability.² Therefore, unstable engine operation is never reached.

In such cases, all the 250 cycles measured on the test bench were grouped in four clusters, namely misfiring cycles, slow cycles, fast cycles, and knocking cycles.

The gross HRR traces for each of these clusters are depicted in Figure 5, for $\lambda = 1.0$ and 1.4.

As expected, for every cluster the maximum HRR is lower for $\lambda = 1.4$ than for $\lambda = 1.0$. There are no misfiring cycles detected for $\lambda = 1.0$, confirming the lowest COV_{IMEP} observed in this case, while few cases with misfire were detected for $\lambda = 1.4$, due to the combustion slowdown for leaner mixtures. On the other hand, there are more knocking cycles in the test cases with $\lambda = 1.0$ than for $\lambda = 1.4$, confirming the higher MAPO value in stoichiometric conditions (Table 4). In both cases, the knocking cycles are characterized by a second peak of HRR after the main one, indicating the combustion of the end-gases. Particularly, for a few cycles, this second peak is higher in the case with $\lambda = 1.4$ than in the stoichiometric one, indicating strong knocking combustion events. In both cases ($\lambda = 1.0$ and 1.4), most cycles are characterized by regular combustion, so they were in the slow and fast-burning clusters. Particularly, there are more slow cycles in the case with $\lambda = 1.4$ than in the stoichiometric one, due to the slower combustion in the former case.

Impact of the air-fuel ratio. Once the 250 cycles are clustered, the impact of the air-fuel ratio on the CCV is assessed by allocating each cycle in one of the four clusters for different λ values.

In Table 5 the probability matrices of each cluster, as described in Section 3.3, are reported for $\lambda = 1.0$ and 1.4.

The probability matrix for $\lambda = 1.0$ evidences that there is no probability of misfiring cycles, confirming what is observed in Figure 5. On the other hand, for $\lambda = 1.4$, it is worth noting that there is a 100% probability of knocking combustion in the current cycle if there is a misfire in the previous one. This is due to the excess of unburned fuel from the misfiring cycle, which burns all at once causing abnormal combustion. In both cases, the most frequent cycles are the fast-burning ones. In fact, for $\lambda = 1.0$ there is a 54% probability of a fast cycle if the previous cycle is slow-burning and a 59% if the previous one is fast-burning. For $\lambda = 1.4$, these percentages are similar to those obtained for $\lambda = 1.0$ (53% and 58%, respectively), evidencing the benefit of the passive prechamber of promoting a stable combustion process also under lean mixture engine operation.

The 250 cycles allocated in the four clusters, together with their distribution, are represented in Figure 6(a) and (b) for $\lambda = 1.0$ and 1.4, respectively.

It can be still observed that the fast cycles are the most frequent in both cases. However, the case with $\lambda = 1.4$ is characterized by a greater number of slow cycles, due to the combustion slowdown as the mixture becomes leaner. Furthermore, the higher number of knocking cycles evidences the greater knock tendency of the case with $\lambda = 1.0$, if compared to the case with $\lambda = 1.4$. In fact, for the stoichiometric case, there is a probability of about 18% to have knock if the previous cycle is slow or fast (Table 5), while these probabilities are very low for $\lambda = 1.4$.

As mentioned in Section 3.4, after the validation against the mean cycle of each λ value, further tuning of the combustion model parameters was carried out for each of the four clusters. Figure 7(a)–(d) shows the in-cylinder pressure and net HRR traces obtained from the model simulations for each cluster, in the case of $\lambda = 1.0$ and 1.4.

The parameters' tuning was carried out by slightly varying C_{tfs} and C_{tls} from the values obtained for the mean cycle. Particularly, it can be noted that the stoichiometric case (Figure 7(a) and (b)) is characterized by maximum in-cylinder pressure and HRR similar to each other for the different clusters. On the other hand, the case with $\lambda = 1.4$ exhibits a large increase of maximum pressure and HRR when moving from misfiring cycles to knocking ones, denoting higher variability than the stoichiometric case. However, the faster flame development within the cylinder, promoted by the turbulent jets, ensures stable combustion even in lean-burn conditions, thus reducing the relative importance of CCV compared to a traditional SI concept.^{32,35}

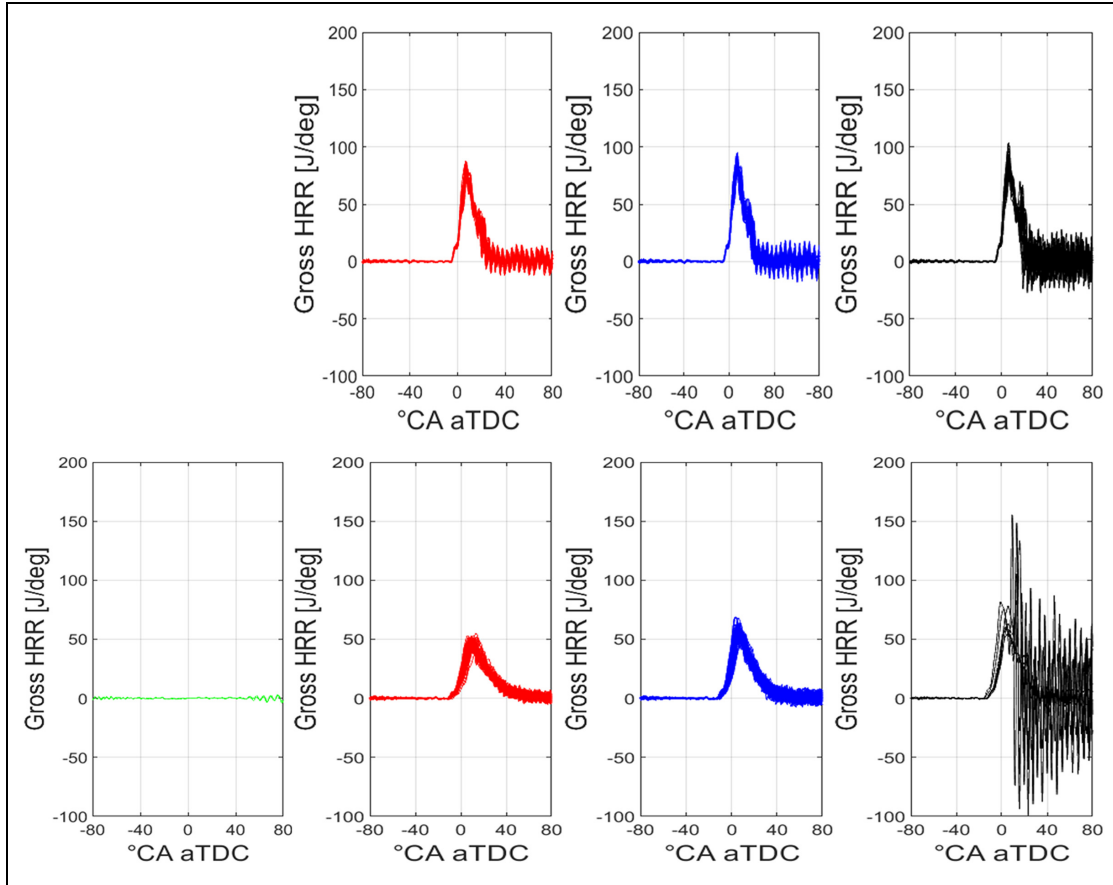


Figure 5. Gross HRR traces of the cycles in the different clusters, for $\lambda = 1.0$ (top) and $\lambda = 1.4$ (bottom).

Table 5. Probability matrices of each cluster computed for $\lambda = 1.0$ (top) and $\lambda = 1.4$ (bottom).

$\lambda = 1.0$	Misfire (current)	Slow cycles (current)	Fast cycles (current)	Knock (current)
Misfire (previous)	0.00	0.00	0.00	0.00
Slow cycles (previous)	0.00	0.28	0.54	0.18
Fast cycles (previous)	0.00	0.23	0.59	0.18
Knock (previous)	0.00	0.32	0.40	0.28
$\lambda = 1.4$	Misfire (current)	Slow cycles (current)	Fast cycles (current)	Knock (current)
Misfire (previous)	0.00	0.0	0.00	1.00
Slow cycles (previous)	0.00	0.47	0.53	0.00
Fast cycles (previous)	0.01	0.38	0.58	0.02
Knock (previous)	0.00	0.71	0.00	0.29

Model simulations were carried out for the different clusters to assess how the CCV impacts on engine performance and combustion process. Particularly, the simulation results were collected for each cluster. Then, simulation results for each cluster were arranged in sequence, according to the cluster chosen for each cycle following the stochastic procedure described in Section 3.3 (Figure 6). Figures 8 and 9(a)–(d) depict the experimental observations of IMEP, maximum in-cylinder pressure and its location and combustion phasing (i.e. CA50) for all the 250 cycles, together with the sequences of the simulation results, for $\lambda = 1.0$ and 1.4.

The IMEP sequences shown in Figures 8(a) and 9(a), evidence the slight disagreement between the mean value of experimental and simulated sequences that is due to the combustion model tuning procedure against the mean cycle, described in Section 4.1. Furthermore, a higher data dispersion can be noticed when λ is increased from 1.0 to 1.4, confirmed by a higher range of the distributions of both experimental and clustering results (Figures 8(a) and 9(a), right). The two lowest IMEP values in the case of $\lambda = 1.4$ (Figure 9(a)), noticeable from both experimental and simulated sequences, correspond to the two misfiring cycles

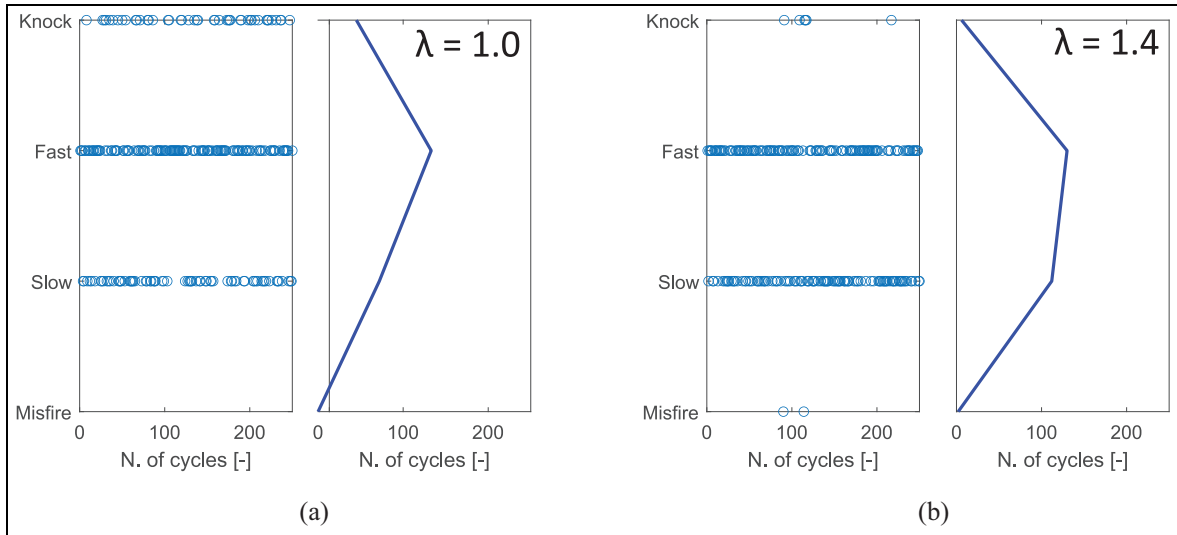


Figure 6. Cycles allocation in the four clusters (blue dots) and their distribution (blue line) for $\lambda = 1.0$ (a) and $\lambda = 1.4$ (b).

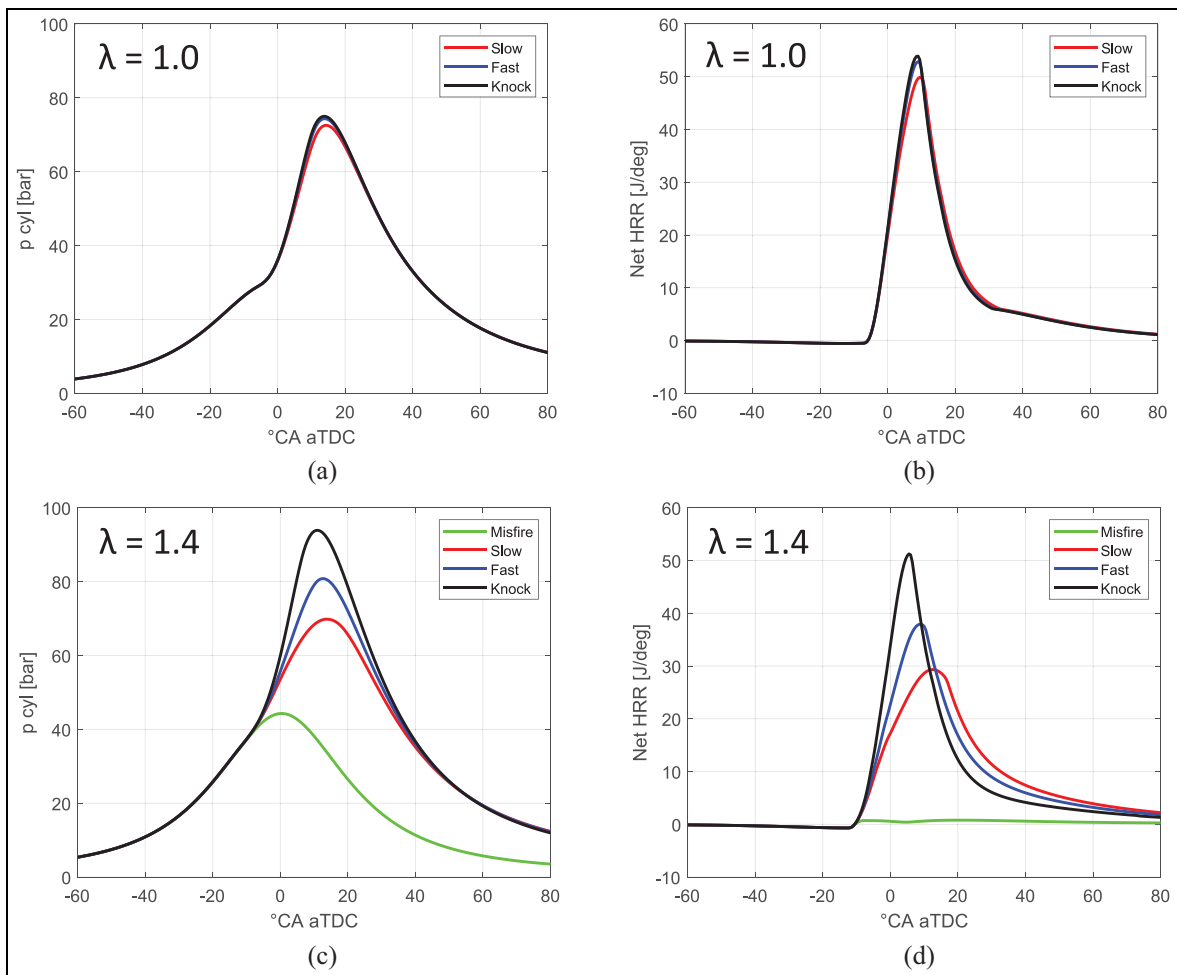


Figure 7. (a–d) Simulated in-cylinder pressure and net HRR traces for the different clusters, at $\lambda = 1.0$ and 1.4.

detected. However, it is worth noting that the number of misfires at $\lambda = 1.4$ is very low if compared to a conventional SI system, thanks to the faster flame propagation promoted by the passive TJI concept.^{32,35}

The increasing influence of CCV for higher air-fuel ratios is noticeable also from both sequences and distributions of maximum in-cylinder pressure (Figures 8(b) and 9(b)). Particularly, the distribution of the simulated

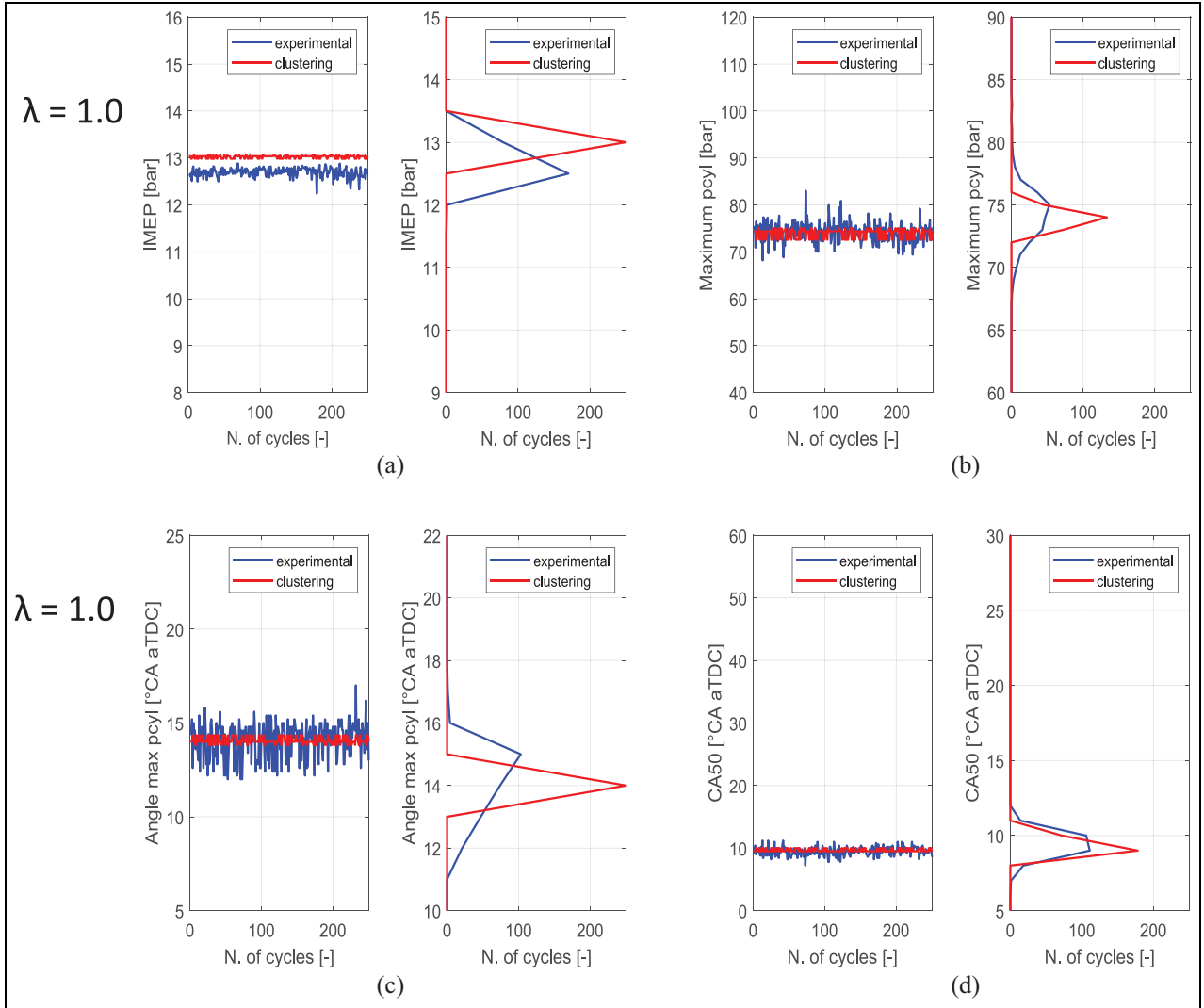


Figure 8. Comparison between experimental observations and clustering results for all 250 cycles of IMEP (a), max in-cyl. pressure (b), angle of max pressure (c), and CA50 (d), for $\lambda = 1.0$.

cycles for $\lambda = 1.4$ (Figure 9(b), right) is characterized by two modes not clearly identifiable in the stoichiometric case, corresponding to the slow (lower value) and fast (higher value) cycles, respectively.

Concerning the angle of maximum pressure (Figures 8(c) and 9(c)), the mean value is slightly lower for the case with $\lambda = 1.4$, given the higher value of the spark advance in such case. However, the higher data dispersion, together with the wider distribution, confirms the higher relative importance assumed by CCV as λ increases. Such increasing in data dispersion is confirmed in both experimental and simulated CA50 sequences for $\lambda = 1.0$ and 1.4 (Figures 8(d) and 9(d), left). Particularly, the two peaks in both experimental and simulated sequences coincide with the two misfiring cycles detected for $\lambda = 1.4$. It is interesting to note how the approach adopted can reproduce the knocking cycles following the misfires, confirming what was stated above. This aspect is particularly evident from the sequences of maximum in-cylinder pressure for $\lambda = 1.4$ (Figure 9(b)). A misfiring cycle, identified by a

very low maximum pressure, is followed by a knock, which instead is identified by a peak of maximum pressure.

Furthermore, observing the comparison between the distributions obtained from the experimental results and the clustering procedure (Figures 8(d) and 9(d), right), it can be noted that they are centered at about the same value in the case of $\lambda = 1.0$. On the other hand, the simulated CA50 distribution in the case of $\lambda = 1.4$ experiences two modes, as observed for the maximum pressure distribution (Figure 9(b), right). Particularly, in such case, a slightly higher number of fast cycles (lower CA50 value) is noticeable, confirming the higher probability of this cluster (Table 5).

CCV prediction. In addition to the test cases with $\lambda = 1.0$ and 1.4 , the CCV analysis was carried out also in the case with $\lambda = 1.2$. The reason lies in the fact that such a case is characterized by a COV_{IMEP} between those recorded in the two cases previously analyzed (see

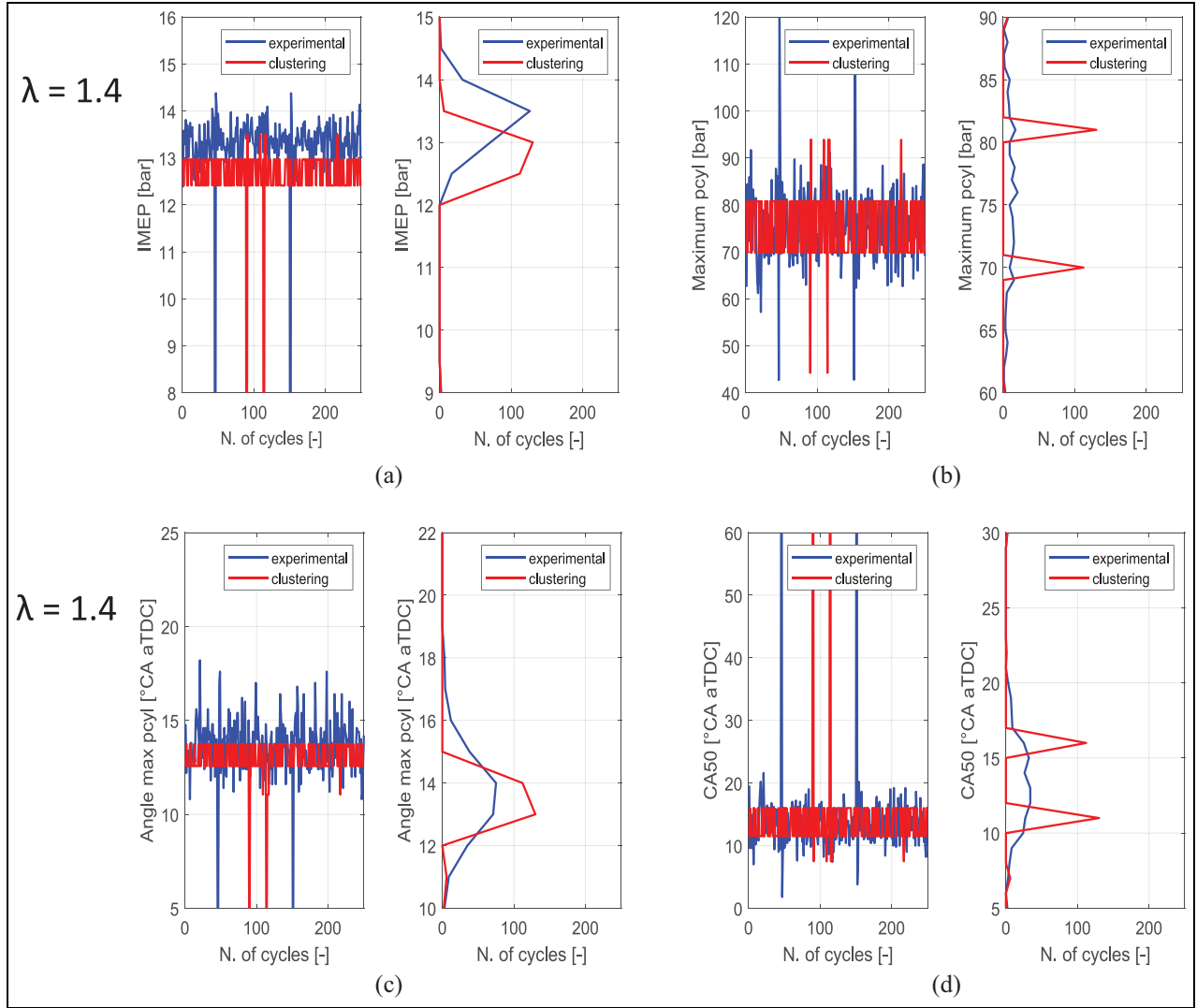


Figure 9. Comparison between experimental observations and clustering results for all 250 cycles of IMEP (a), max in-cyl. pressure (b), angle of max pressure (c), and CA50 (d), for $\lambda = 1.4$.

Table 6. Estimated probability matrix of each cluster for $\lambda = 1.2$.

$\lambda = 1.2$	Misfire (current)	Slow cycles (current)	Fast cycles (current)	Knock (current)
Misfire (previous)	0.00	0.00	0.00	1.00
Slow cycles (previous)	0.00	0.37	0.53	0.09
Fast cycles (previous)	0.01	0.31	0.59	0.10
Knock (previous)	0.00	0.52	0.20	0.28

Table 4). To appreciate the prediction accuracy of the method, the CCV for $\lambda = 1.2$ was assessed starting from the data obtained in the cases with $\lambda = 1.0$ and 1.4. In particular, the probability matrix for $\lambda = 1.2$ (Table 6) was calculated by linearly interpolating the values obtained for the two other cases and the clusters were chosen for all the cycles according to the same procedure, described in Section 3.3.

Like the case with $\lambda = 1.4$, also for $\lambda = 1.2$, there is a 100% probability of knocking in the current cycle if a misfire occurs in the previous one. Moreover, also in

this case, the most frequent cycles are the fast-burning ones. In fact, there is a 53% probability of a fast cycle if the previous cycle is slow-burning and a 59% if the previous one is fast-burning.

The result of the cycles' allocation in the different clusters for $\lambda = 1.2$ is shown in Figure 10.

As it can be observed, the proposed method allows estimating high frequencies in the slow and fast cycles but leads to an overestimation with respect to the values obtained by the experimental measurements (red line), while the number of knocking cycles is underestimated

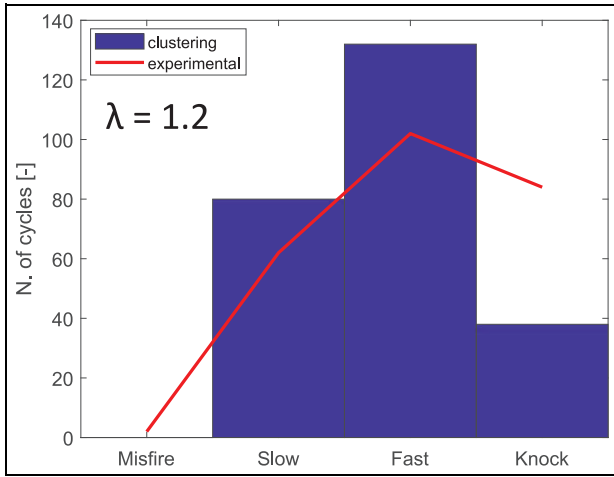


Figure 10. Comparison of the cycles' allocation in the different clusters with the experimental observations, for $\lambda = 1.2$.

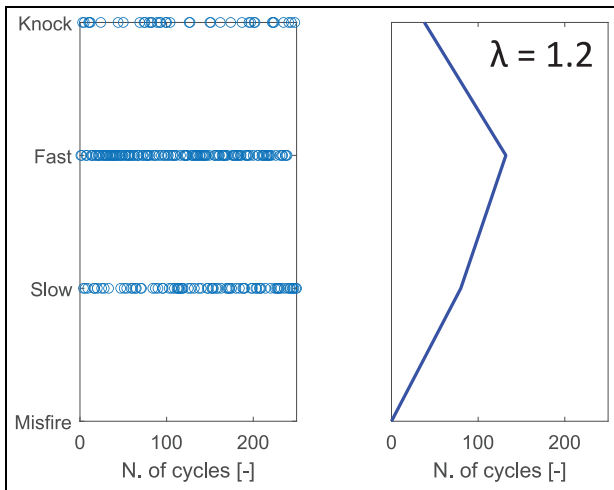


Figure 11. Cycles allocation in the four clusters (blue dots) and their distribution (blue line) for $\lambda = 1.2$.

by the cycles' allocation according to the probability matrix in Table 6. The number of misfires is underestimated since no misfire is experienced at $\lambda = 1.2$ according to the proposed method, while experimental results show two misfires in the 250 cycles. The deviations between the estimated and measured distribution lie in the fact that the CCV does not linearly depend on λ , as assumed by the proposed method.

The 250 cycles allocated in the four clusters for $\lambda = 1.2$, together with their distribution, are shown in Figure 11.

As observed for the other two cases, also for $\lambda = 1.2$ the fast cycles are the most frequent, confirming what is reported in Table 6. Furthermore, as expected, the number of knocking cycles for $\lambda = 1.2$ is between the values obtained for $\lambda = 1.0$ – 1.4 , as well as the slow-burning cycles.

Also in this case, model simulation results were collected and arranged in sequence to assess the relative

importance of CCV. Figure 12(a)–(d) shows the sequences of both experimental and simulated IMEP, maximum in-cylinder pressure and its location, and CA50 for all 250 cycles, together with their distributions, for $\lambda = 1.2$.

The results show a good agreement between the experimental and simulated IMEP distribution (Figure 12(a), right), especially in predicting the mean value. However, if the probability matrix is computed starting from the values of the other two cases, this approach is not able to reproduce the two misfiring cycles detected by the experimental observations (Figure 12(a), left). The same model accuracy in predicting the mean value is noticeable also in the maximum pressure sequences (Figure 12(b), left). Particularly, in this case, three levels of maximum pressure are distinguishable in the simulated sequence, which are reflected in as many modes of the simulated maximum pressure distribution. These modes are representative of slow, fast, and knocking cycles. Also from this distribution, it is evident that fast cycles are the most frequent for $\lambda = 1.2$.

The experimental and simulated maximum pressure angle sequences (Figure 12(c), left) exhibit a data dispersion for $\lambda = 1.2$, which is higher than $\lambda = 1.0$ but lower than $\lambda = 1.4$, as expected. Also in this case, three levels are distinguishable from the simulated sequence, corresponding to slow (higher values), fast (medium values), and knocking cycles (lower values). On the other hand, the simulated distribution of the maximum pressure angle (Figure 12(c), right) seems to be less wide than the experimental one, which features about three modes.

Concerning the combustion phasing (Figure 12(d)), the case with $\lambda = 1.2$ experiences a very low data dispersion, as observed for $\lambda = 1.0$ (Figure 8(d)), together with good accuracy of the model in predicting the mean value.

From the comparison between the experimental observations and the clustering results for $\lambda = 1.2$, good accuracy in assessing the relative importance of CCV is evident, despite the differences in the cycles' number for each cluster observed in Figure 10. Therefore, the approach adopted to cluster the experimental data and then to allocate the cycles in the different clusters seems to be reliable also in cases where no experimental data is available.

Conclusions and future developments

The paper deals with the experimental and numerical investigation of the effects of a passive TJI system on SI engines' performance, in stoichiometric and lean-burn operating conditions. A 1-D engine model was developed and validated against the experimental data to simulate the TJI combustion process. Based on 1-D model results, a stochastic methodology was applied to predict the CCV depending on the current relative air-fuel ratio, ranging from 1.0 to 1.6.

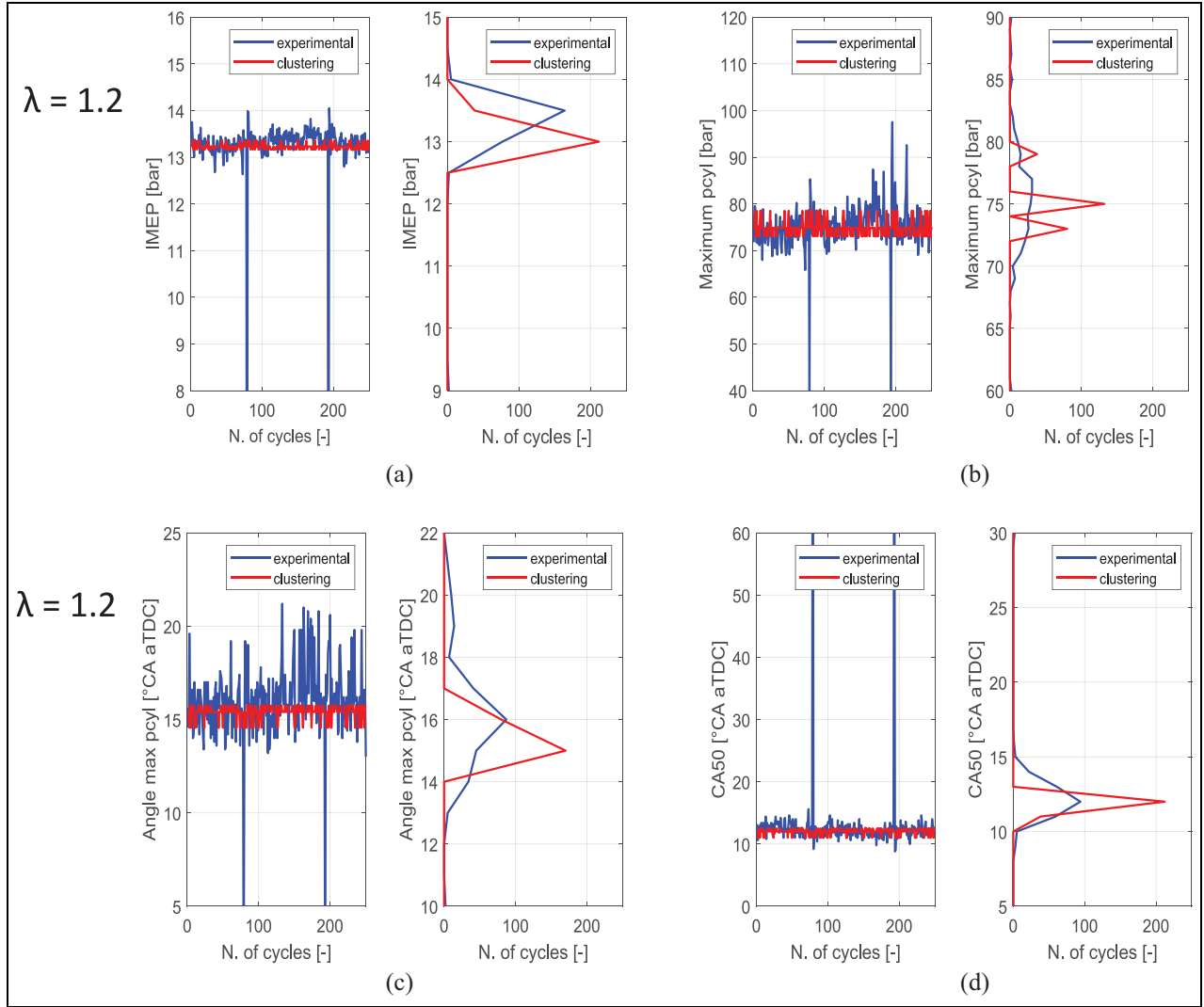


Figure 12. Comparison between experimental observations and clustering results for all 250 cycles of IMEP (a), max in-cyl. pressure (b), angle of max pressure (c), and CA50 (d), for $\lambda = 1.2$.

Both experimental data and simulation results evidence that an increase of λ results in a combustion slowdown, noticeable from the decrease of maximum HRR as λ is increased from 1.0 to 1.6. However, the adoption of a passive TJI concept allows guaranteeing a faster combustion process compared to a conventional spark ignition system, particularly in the case of lean mixture.

Afterward, the influence of mixture leaning on CCV was assessed, starting from the cases with $\lambda = 1.0$ and 1.4, as they experience the lowest and the highest variability, respectively. As expected, increasing λ from 1.0 to 1.4 results in an increase of misfiring cycles, which are absent in the stoichiometric case, and in a reduction of the knocking cycles. Moreover, in the case of $\lambda = 1.4$, a 100% probability of a knocking cycle after a misfire is observed. In both cases, fast-burning cycles are the most frequent although the case with $\lambda = 1.4$ exhibits a greater number of slow cycles, due to the combustion slowdown as the mixture becomes leaner.

The stochastic allocation of the cycles in the four clusters allows estimating the sequences of the main metrics of the combustion process, namely IMEP, maximum in-cylinder pressure and its location, and CA50, starting from 1-D simulation results. Particularly, a higher data dispersion is observed for the IMEP sequences when λ is increased from 1.0 to 1.4. This trend indicates higher relative importance of CCV as the mixture is leaned out and is confirmed by the sequence and the distribution of maximum in-cylinder pressure and CA50.

In addition to cases with $\lambda = 1.0$ and 1.4, the CCV analysis was also carried out for the case with $\lambda = 1.2$. In such case, the probability matrix was calculated by linearly interpolating the values of the two other cases, to assess the prediction of the method even in case of lack of experimental data. Like the case with $\lambda = 1.4$, 100% probability of knocking after a misfiring is observed. Moreover, the analysis of the sequences of the most relevant combustion metrics exhibits a good

agreement between experimental data and clustering results, thus confirming the reliability of the proposed stochastic method to predict the CCV, even in case no experimental data are available.



Declaration of conflicting interests


The author(s) declared no potential conflicts of interest with respect to the research, authorship, and/or publication of this article.

Funding

The author(s) received no financial support for the research, authorship, and/or publication of this article.

ORCID iDs

Emmanuele Frasci  <https://orcid.org/0000-0003-1010-9635>
Ricardo Novella Rosa  <https://orcid.org/0000-0002-5123-6924>

Benjamín Plá Moreno  <https://orcid.org/0000-0001-9238-2939>

References

1. Vressner A, Gabrielson P, Gekas I and Senar-Serra E. Meeting the EURO VI NO_x emission legislation using a EURO IV base engine and a SCR/ASC/DOC/DPF configuration in the world harmonized transient cycle, <https://doi.org/10.4271/2010-01-1216>. Accessed in July 2022.
2. Heywood JB. *Internal combustion engine fundamentals*. New York, NY: McGraw-Hill Book Co, 1988.
3. Attard WP, Konidaris S, Hamori F, Toulson E and Watson HC. Compression ratio effects on performance, efficiency, emissions and combustion in a carbureted and PFI small engine. SAE technical paper 2007-01-3623, 2007. <https://doi.org/10.4271/2007-01-3623>. Accessed July 2022.
4. Novella R, Pla B, Bares P and Jiménez I. Acoustic characterization of combustion chambers in reciprocating engines: an application for low knocking cycles recognition. *Int J Engine Res* 2022; 23(1): 120–131.
5. Attard WP and Parsons P. Flame kernel development for a spark initiated pre-chamber combustion system capable of high load, high efficiency and near zero NO_x emissions. *SAE Int J Engines* 2010; 3(2): 408–427.
6. Wang J, Chen H, Hu Z, Yao M and Li Y. A review on the Pd-based three-way catalyst. *Catal Rev* 2015; 57(1): 79–144.
7. Irimescu A, Merola S and Martinez S. Influence of engine speed and injection phasing on lean combustion for different dilution rates in an optically accessible wall-guided spark ignition engine. *SAE Int J Engines* 2018; 11(6): 1343–1369.
8. Attard WP and Blaxill H. A lean burn gasoline fueled pre-chamber jet ignition combustion system achieving high efficiency and low NO_x at part load. SAE technical paper 2012-01-1146, 2012. <https://doi.org/10.4271/2012-01-1146>. Accessed in August 2022.
9. Peterson B, Reuss DL and Sick V. On the ignition and flame development in a spray-guided direct-injection spark-ignition engine. *Combust Flame* 2014; 161(1): 240–255.
10. Gentz G, Thelen B, Gholamisheeri M, et al. A study of the influence of orifice diameter on a turbulent jet ignition system through combustion visualization and performance characterization in a rapid compression machine. *Appl Therm Eng* 2015; 81: 399–411.
11. d'Adamo A, Breda S, Berni F and Fontanesi S. Understanding the origin of cycle-to-cycle variation using large-eddy Simulation: similarities and differences between a homogeneous Low-Revving speed research engine and a production DI turbocharged engine. *SAE Int J Engines* 2018; 12(1): 45–56.
12. Maldonado BP and Kaul BC. Control-oriented modeling of cycle-to-cycle combustion variability at the misfire limit in SI engines. In: *Proceedings of the ASME 2020 Dynamic systems and control conference*, Pittsburgh, PA, USA, 4–7 October 2020. American Society of Mechanical Engineers, USA.
13. Maldonado BP, Zaseck K, Kitagawa E and Stefanopoulou AG. Closed-loop control of combustion initiation and combustion duration. *IEEE Trans Control Syst Technol* 2020; 28(3): 936–950.
14. Pla B, De la Morena J, Bares P and Jiménez I. Cycle-to-cycle combustion variability modelling in spark ignited engines for control purposes. *Int J Engine Res* 2020; 21(8): 1398–1411.
15. Toulson E, Schock HJ and Attard WP. A review of pre-chamber initiated jet ignition combustion systems. SAE technical paper 2010-01-2263, 2010.
16. Alvarez CEC, Couto GE, Roso VR, Thiriet AB and Valle RM. A review of prechamber ignition systems as lean combustion technology for SI engines. *Appl Therm Eng* 2018; 128: 107–120.
17. Sementa P, Catapano F, Di Iorio S and Vaglieco BM. Experimental investigation of a fueled prechamber combustion in an optical small displacement SI methane engine. SAE technical paper 2019-24-0170, 2019.
18. Assanis D, Engineer N, Neuman P and Wooldridge M. Computational development of a dual pre-chamber engine concept for lean burn combustion. SAE technical paper 2016-01-2242, 2016.
19. Attard WP, Bassett M, Parsons P and Blaxill H. A new combustion system achieving high drive cycle fuel economy improvements in a modern vehicle powertrain. SAE technical paper 2011-01-0664, 2011.
20. Gentz G, Thelen B, Litke P, Hoke J and Toulson E. Combustion visualization, performance, and CFD modeling of a pre-chamber turbulent jet ignition system in a rapid compression machine. *SAE Int J Engines* 2015; 8(2): 538–546.
21. Gentz G, Gholamisheeri M and Toulson E. A study of a turbulent jet ignition system fueled with iso-octane: pressure trace analysis and combustion visualization. *Appl Energy* 2017; 189: 385–394.
22. Chinnathambi P, Bunce M and Cruff L. RANS based multidimensional modeling of an ultra-lean burn pre-chamber combustion system with auxiliary liquid gasoline injection. SAE technical paper 2015-01-0386, 2015.
23. Biswas S, Tanvir S, Wang H and Qiao L. On ignition mechanisms of premixed CH₄/air and H₂/air using a hot turbulent jet generated by pre-chamber combustion. *Appl Therm Eng* 2016; 106: 925–937.
24. Allison PM, de Oliveira M, Giusti A and Mastorakos E. Pre-chamber ignition mechanism: experiments and simulations on turbulent jet flame structure. *Fuel* 2018; 230: 274–281.

25. Attard WP and Blaxill H. A single fuel pre-chamber jet ignition powertrain achieving high load, high efficiency and near zero NO_x emissions. *SAE Int J Engines* 2011; 5(3): 734–746.
26. Attard WP, Blaxill H, Anderson EK and Litke P. Knock limit extension with a gasoline fueled pre-chamber jet igniter in a modern vehicle powertrain. *SAE Int J Engines* 2012; 5(3): 1201–1215.
27. Attard WP, Toulson E, Huisjen A, Chen X, Zhu G and Schock H. Spark ignition and pre-chamber turbulent jet ignition combustion visualization. SAE technical paper 2012-01-0823, 2012.
28. Attard WP, Fraser N, Parsons P and Toulson E. A turbulent jet ignition pre-chamber combustion system for large fuel economy improvements in a modern vehicle powertrain. *SAE Int J Engines* 2010; 3(2): 20–37.
29. Vedula RT, Gentz G, Stuecken T, Toulson E and Schock H. Lean burn combustion of iso-octane in a rapid compression machine using dual mode turbulent jet ignition system. *SAE Int J Engines* 2018; 11(1): 95–107.
30. Frasci E, Sementa P, Arsie I, Jannelli E and Vaglieco BM. Experimental and numerical investigation of a lean SI engine to be operated as range extender for hybrid powertrains. SAE technical paper 2021-24-0005, 2021.
31. Novella R, Pla B, Bares P and Aramburu A. Identification of adequate combustion in turbulent jet ignition engines using machine learning algorithms. *IFAC-PapersOnLine* 2021; 54(10): 102–107.
32. Benajes J, Novella R, Gomez-Soriano J, Martinez-Hernandez PJ, Libert C and Dabiri M. Evaluation of the passive pre-chamber ignition concept for future high compression ratio turbocharged spark-ignition engines. *Appl Energy* 2019; 248: 576–588.
33. GT-Suite Engine performance application manual, Gamma Technologies.
34. Wenig M, Roggendorf K and Fogla N. Towards predictive dual-fuel combustion and prechamber modeling for large two-stroke engines in the scope of 0D/1D simulation. In *Proceedings of the 29th CIMAC world congress on combustion engine technology*, Vancouver, BC, Canada, 10–14 June 2019, pp.10–14.
35. Novella R, Pastor J, Gomez-Soriano J, et al. Experimental and numerical analysis of passive pre-chamber ignition with EGR and air dilution for future generation passenger car engines. SAE technical paper 2020-01-0238, 2020.
36. Ouellette P and Hill PG. Turbulent transient gas injections. *J Fluid Eng* 2000; 122(4): 743–752.
37. Wahiduzzaman S, Moral T and Sheard S. Comparison of measured and predicted combustion characteristics of a four-valve SI engine. *SAE technical paper* 930613, 1993.
38. Irimescu A, Catapano F, Di Iorio S, Merola S, Sementa P and Vaglieco BM. Quasi-dimensional simulation of downsizing and inverter application for efficient part load operation of spark ignition engine driven micro-cogeneration systems. SAE technical paper 2018-32-0061, 2018.
39. Fogla N, Bybee M, Mirzaeian M, Millo F and Wahiduzzaman S. Development of a K-k-ε phenomenological model to predict in-cylinder turbulence. *SAE Int J Engines* 2017; 10(2): 562–575.
40. Woschni G. A universally applicable equation for the instantaneous heat transfer coefficient in the internal combustion engine. SAE technical paper 670931, 1967.
41. Lloyd S. Least squares quantization in PCM. *IEEE Trans Inf Theory* 1982; 28(2): 129–137.
42. Ahmed M, Seraj R and Islam SMS. The k-means algorithm: a comprehensive survey and performance evaluation. *Electronics* 2020; 9(8): 1295.
43. Naber J, Blough JR, Frankowski D, Goble M and Szpytman JE. Analysis of combustion knock metrics in spark-ignition engines. SAE technical paper 2006-01-0400, 2006.

Appendix

Abbreviations

CA50	Crank angle of 50% of burned fuel
CCV	Cycle-to-cycle variability
CI	Compression ignition
DOHC	Double over head camshaft
EGR	Exhaust gas recirculation
FSN	Filter smoke number
GDI	Gasoline direct injection
HRR	Heat release rate
IMEP	Indicated mean effective pressure
MAPO	Maximum amplitude of pressure oscillation
PFI	Port fuel injection
SI	Spark ignition
SOC	Start of combustion
TDC	Top dead center
TJI	Turbulent jet ignition
TWC	Three-way catalyst

Greek letters

γ	Ratio of specific heats
λ	Relative air-fuel ratio
ρ	Density
τ	Characteristic timescale of the flame propagation